NASA/TM-20210017582

Comparing Commercial and Research Computational Fluid Dynamic Codes Using High-Order Workshop Benchmark Problems

David J. Friedlander
Glenn Research Center, Cleveland, Ohio

Carl Leake
Embry-Riddle Aeronautical University, Prescott, Arizona

Amy Zhou
University of Michigan, Ann Arbor, Michigan

Xiao-Yen Wang and H. T. Huynh
Glenn Research Center, Cleveland, Ohio

September 2021

NASA STI Program . . . in Profile

Since its founding, NASA has been dedicated to the advancement of aeronautics and space science. The NASA Scientific and Technical Information (STI) Program plays a key part in helping NASA maintain this important role.

The NASA STI Program operates under the auspices of the Agency Chief Information Officer. It collects, organizes, provides for archiving, and disseminates NASA's STI. The NASA STI Program provides access to the NASA Technical Report Server—Registered (NTRS Reg) and NASA Technical Report Server—Public (NTRS) thus providing one of the largest collections of aeronautical and space science STI in the world. Results are published in both non-NASA channels and by NASA in the NASA STI Report Series, which includes the following report types:

- TECHNICAL PUBLICATION. Reports of completed research or a major significant phase of research that present the results of NASA programs and include extensive data or theoretical analysis. Includes compilations of significant scientific and technical data and information deemed to be of continuing reference value. NASA counter-part of peer-reviewed formal professional papers, but has less stringent limitations on manuscript length and extent of graphic presentations.

- TECHNICAL MEMORANDUM. Scientific and technical findings that are preliminary or of specialized interest, e.g., "quick-release" reports, working papers, and bibliographies that contain minimal annotation. Does not contain extensive analysis.

- CONTRACTOR REPORT. Scientific and technical findings by NASA-sponsored contractors and grantees.

- CONFERENCE PUBLICATION. Collected papers from scientific and technical conferences, symposia, seminars, or other meetings sponsored or co-sponsored by NASA.

- SPECIAL PUBLICATION. Scientific, technical, or historical information from NASA programs, projects, and missions, often concerned with subjects having substantial public interest.

- TECHNICAL TRANSLATION. English-language translations of foreign scientific and technical material pertinent to NASA's mission.

For more information about the NASA STI program, see the following:

- Access the NASA STI program home page at http://www.sti.nasa.gov

- E-mail your question to help@sti.nasa.gov

- Fax your question to the NASA STI Information Desk at 757-864-6500

- Telephone the NASA STI Information Desk at 757-864-9658

- Write to:
  NASA STI Program
  Mail Stop 148
  NASA Langley Research Center
  Hampton, VA 23681-2199

NASA/TM-20210017582

Comparing Commercial and Research Computational Fluid Dynamic Codes Using High-Order Workshop Benchmark Problems

David J. Friedlander
Glenn Research Center, Cleveland, Ohio

Carl Leake
Embry-Riddle Aeronautical University, Prescott, Arizona

Amy Zhou
University of Michigan, Ann Arbor, Michigan

Xiao-Yen Wang and H. T. Huynh
Glenn Research Center, Cleveland, Ohio

National Aeronautics and
Space Administration

Glenn Research Center
Cleveland, Ohio 44135

September 2021

Acknowledgments

The authors would like to thank the NASA Transformative Aeronautics Concepts Program, Transformational Tools and Technologies Project for funding and the NASA's High-End Computing Program for providing super-computing resources. The authors would also like to thank Q. Lu and Dr. Z. J. Wang of the University of Kansas for providing the FR results for the vortex problem and Dr. Z. J. Wang for providing the FR results for the flat plate problem. Furthermore, the authors would like to thank C. Peters from the NASA Glenn Research Center for providing the MATLAB® (The Mathworks, Inc.) code to generate the Blasius solution *u* velocity profiles for the flat plate problem.

This report contains preliminary findings, subject to revision as analysis proceeds.

This work was sponsored by the Transformative Aeronautics Concepts Program.

Level of Review: This material has been technically reviewed by technical management.

Available from

NASA STI Program
Mail Stop 148
NASA Langley Research Center
Hampton, VA 23681-2199

National Technical Information Service
5285 Port Royal Road
Springfield, VA 22161
703-605-6000

This report is available in electronic form at http://www.sti.nasa.gov/ and http://ntrs.nasa.gov/

Comparing Commercial and Research Computational Fluid Dynamic Codes Using High-Order Workshop Benchmark Problems

David J. Friedlander
National Aeronautics and Space Administration
Glenn Research Center
Cleveland, Ohio 44135

Carl Leake
Embry-Riddle Aeronautical University
Prescott, Arizona 86301

Amy Zhou
University of Michigan
Ann Arbor, Michigan 48109

Xiao-Yen Wang and H. T. Huynh
National Aeronautics and Space Administration
Glenn Research Center
Cleveland, Ohio 44135

Abstract

The commercial computational fluid dynamic (CFD) code ANSYS Fluent and multiple research CFD codes (ez4d which uses the conservation element and solution element (CESE) method and codes that use the flux reconstruction (FR) method) were tested using three different benchmark problems from the International Workshop for High-Order CFD Methods. The benchmark problems included the transonic Ringleb flow, vortex transport by uniform flow, and laminar boundary layer on a flat plate. Simulation results from the benchmark problems that had ez4d solutions showed that the Fluent solutions had less error than the ez4d solutions for a given degree of freedom. As expected, both the Fluent and ez4d solutions had larger errors for a given degree of freedom than the simulations that used the FR method because both Fluent and ez4d utilized a second-order scheme whereas the FR codes utilized a fourth-order scheme.

Nomenclature

A	area
c_d	drag coefficient
c_f	skin friction coefficient
h	length scale
J	Ringleb parameter
k	streamline parameter
L	characteristic length
n	number

O	numerical scheme order
p	pressure
q	velocity magnitude
R	specific gas constant
Re_x	axial Reynolds number
s	entropy
T	temperature
t	time
u, v	streamwise and transverse velocity components
x, y	cartesian coordinates
Δy_{wall}	wall-normal spacing
β	vortex strength
δ	boundary-layer thickness
γ	ratio of specific heats
ρ	density

Subscripts:

GL	current grid level
∞	freestream

1.0 Introduction

There is a push in the computational fluid dynamic (CFD) arena to develop CFD codes with higher accuracy while maintaining a relatively quick turn-around time in obtaining solutions. This push for higher accuracy has led to the development of several high-order research codes, including codes that are unstructured in nature. High-order refers to numerical schemes that are greater than second-order accurate. A set of CFD benchmark problems have been proposed to test high-order CFD codes, with results shared at the International Workshop for High-Order CFD Methods (Ref. 1). The workshop has been held five times since its inception in 2012. Most submissions to the workshops have been high-order solutions with a lack of low-order solutions to compare to. To help fill this solution gap, the authors decided to run a commercially available CFD code to compare its results to results from research codes. This paper presents the CFD results for three benchmark problems: transonic Ringleb flow, vortex transport by uniform flow, and laminar boundary layer on a flat plate. For comparison, each benchmark problem was simulated using several different codes: ANSYS Fluent, a research code utilizing the conservation element and solution element (CESE) numerical method, and research codes utilizing the flux reconstruction (FR) numerical method.

2.0 Numerical Code Overviews

2.1 ANSYS Fluent

ANSYS Fluent Version 17.2 (Ref. 2) was the commercial CFD solver chosen for this study because of its popularity throughout industry and academia. Information from the Fluent website[1] shows that the software's popularity is due to its versatility: from designing and analyzing race cars to designing and analyzing water turbines. Fluent can use either a pressure- or density-based coupled solver and contains

[1]https://www.ansys.com/products/fluids/ansys-fluent

several numerical schemes, including the Roe-FDS flux (Ref. 3), Green-Gauss node-based spatial gradient (Ref. 4), and the 2nd-order upwind spatial flow schemes that were used in the simulations presented in this paper. In addition, Fluent also allows users to create user-defined functions that allow the utilization of new and personalized models alongside the functions that are already within the software. With its connection and integration into ANSYS Workbench, the user is able to utilize and connect to many major computer aided design systems and complete all CFD components (i.e., geometry generation through post-processing) in one software package. Additional information on the full set of built-in functions and numerical schemes in Fluent can be found in the ANSYS Fluent Theory Guide (Ref. 5).

2.2 Conservation Element and Solution Element (CESE) Method

The CESE method, developed by S.-C. Chang (Refs. 6 and 7) in 1995, is a time accurate formulation with flux-conservation in both space and time. The method treats the discretized derivatives of space and time identically and utilizes a staggered mesh approach consisting of conservation elements (CE) and solution elements (SE). Originally developed as a second-order method, the CESE framework has been extended to higher orders (Ref. 8). The research code ez4d, developed by C.-L. Chang (Ref. 9), is an unstructured Navier-Stokes flow solver that utilizes the CESE numerical method. The code can run both the second-order accurate and the fourth-order accurate versions of the CESE scheme (Ref. 10), although only the second-order accurate scheme was used in this work.

2.3 Flux Reconstruction (FR) Method

The flux reconstruction approach, introduced by H. T. Huynh in 2007 (Ref. 11), provides a simple and economic framework to derive high-order numerical schemes for conservation laws. As used here, economic refers to the easiness of coding the numerical scheme as well as the cost efficiency of running the code. The main idea for the case of one spatial dimension is the following. The data are represented by a polynomial of degree n in each cell, and these polynomials collectively form a function, which can be and usually is discontinuous across cell interfaces. At each interface, the left and right states are used to define a common flux, which is typically the upwind flux. In each cell, the fluxes corresponding to the polynomial data can be approximated by polynomials again of degree n, which are also discontinuous across cell interfaces. These polynomials are called the discontinuous flux function. To resolve the jumps at the cell interface, we reconstruct the flux by a polynomial of degree n+1, which takes on the common flux values at the cell interfaces and thus, is continuous across cells. Such polynomials of degree n+1 are called continuous flux functions. In each cell, it approximates the discontinuous flux function, and different manners of approximation results in different schemes. The FR approach unifies several existing methods: it recovers the discontinuous Galerkin (DG), spectral volume, and spectral difference (or staggered-grid) methods. It also results in numerous new schemes with favorable properties (Ref. 12). While these schemes vary in order-of-accuracy, the fourth-order accurate version of the FR scheme was used in this work.

3.0 Problem Descriptions and Modeling

3.1 Transonic Ringleb Flow

The transonic Ringleb flow problem (Ref. 13), or Ringleb problem for short, involves an inviscid transonic flow through a 2D curved duct-like geometry, shown in Figure 1. For this problem, the Cartesian coordinates are defined as functions of a streamline parameter k and the nondimensional velocity magnitude q, shown in Equations (1) and (2).

$$x(q,k) = \frac{1}{2\rho} \cdot \left(\frac{2}{k^2} - \frac{1}{q^2} \right) - \frac{J}{2} \tag{1}$$

$$y(q,k) = \pm \frac{1}{k\rho q} \cdot \sqrt{1 - \left(\frac{q}{k} \right)^2} \tag{2}$$

where

$$J = \frac{1}{a} + \frac{1}{3a^3} + \frac{1}{5a^5} - \frac{1}{2} \cdot \log\left(\frac{1+a}{1-a} \right) \tag{3}$$

$$\rho = a^{\left(\frac{2}{\gamma - 1} \right)} \tag{4}$$

$$p = \frac{1}{\gamma} \cdot a^{\left(\frac{2\gamma}{\gamma - 1} \right)} \tag{5}$$

$$a = \sqrt{1 - \frac{\gamma - 1}{2} q^2} \tag{6}$$

The left and right boundaries of the duct, modeled as slip walls, were defined by streamlines at $k = 1.5$ and $k = 0.7$, respectively. The top and bottom boundaries of the duct, modeled as a subsonic inflow and outflow respectively, were defined by constant nondimensional velocity magnitudes of 0.5. For use with the Fluent code, which used the density-based solver, three structured 2D grids were generated by modifying the workshop provided P4-cell grids (which utilize high-order quad cells) with equivalent P1-cell grids. For use with the ez4d code, three unstructured 2D grids were created using the Pointwise grid generation software by first creating a structured mesh and then slicing the quadrilaterals into triangles using the "best fit" diagonalize option. Figure 2 shows an example of the diagonalization process. The FR code used the P4-cell grids as provided by the workshop due to the need of higher-order mesh representation. Figure 3 shows example meshes and Table 1 provides a summary of the number of degrees of freedom for all the Ringleb cases. Note that for each code, the number of degrees of freedom, which is a function of the order of the scheme and the number of cells for a cell-based scheme or the number of nodes for a node-based scheme, were increased by increasing the number of cells/nodes within the computational domain.

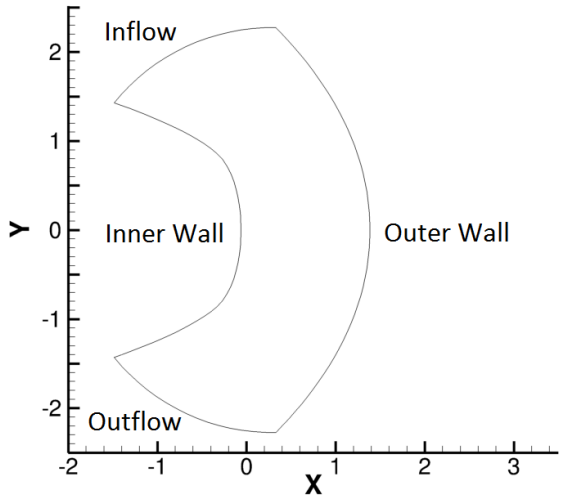

Figure 1.—Ringleb geometry and boundary conditions.

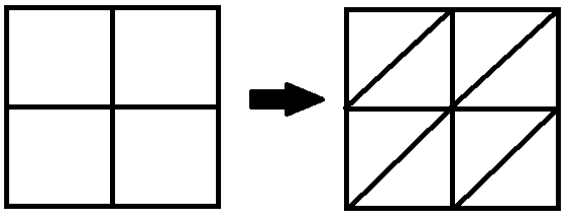

Figure 2.—Example of slicing a quad grid into triangles by diagonalization.

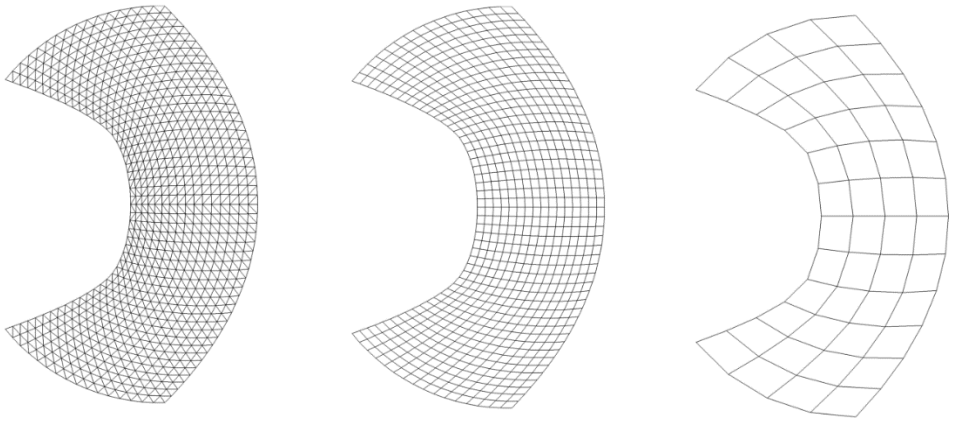

Figure 3.—Example Ringleb grids: ez4d at 6,144 number of degrees of freedom (nDOF) (left), Fluent at 3,072 nDOF (center), and FR at 3,072 nDOF (right).

TABLE 1.—THE NUMBER OF DEGREES OF FREEDOM (NDOF) RUN BY EACH CODE FOR THE RINGLEB PROBLEM

nDOF	Fluent	ez4d	FR
3,072	X	-	X
6,144	-	X	-
12,288	X	-	X
24,576	-	X	-
49,152	X	-	X
98,304	-	X	-

3.2 Vortex Transport by Uniform Flow

The problem of vortex transport by uniform flow (Ref. 14) involves the transport of a vortex within a 2D inviscid flow field. The flow field was bounded by x = 0-0.1 and y = 0-0.1 with the center of the vortex originating at x_c = 0.05 and y_c = 0.05. The vortex was defined by the following perturbations to the freestream flow field:

$$\delta u = \frac{-1 \cdot \left(u_\infty \beta\right) \cdot \left(y - y_c\right) \cdot e^{-0.5r^2}}{0.005} \tag{7}$$

$$\delta v = \frac{\left(u_\infty \beta\right) \cdot \left(x - x_c\right) \cdot e^{-0.5r^2}}{0.005} \tag{8}$$

$$\delta T = \frac{0.5 \cdot \left(u_\infty \beta\right)^2 \cdot e^{-1r^2}}{\frac{\gamma}{\gamma - 1} \cdot R} \tag{9}$$

where

$$r = \frac{\sqrt{\left(x - x_c\right)^2 + \left(y - y_c\right)^2}}{0.005} \tag{10}$$

The simulated vortex had a vortex strength, β, of 0.2 with the freestream flow oriented in only the x-direction at a Mach number of 0.5. The quadrilateral and triangle grids provided by the 3rd International Workshop on High-Order CFD Methods were used for both the Fluent, which used the density-based solver, and the FR code simulations. Sample grids are shown in Figure 4. The intent was to simulate the vortex with the ez4d code; however, simulations are still on-going and will be included in the paper when completed. The FR code hpMusic (Ref. 15) was used in lieu of the FR code that was used in the Ringleb problem due to that the authors were no longer funded to continue the research. The number of degrees of freedom run for the three codes are listed in Table 2. Just like with the Ringleb problem, the number of degrees of freedom per code were increased by increasing the cell count of each grid. Because periodic boundary conditions are used for all boundaries, this problem can be run indefinitely, with one period of time defined as the amount of time it takes for the vortex to propagate from its initial location through the domain and back to its initial location.

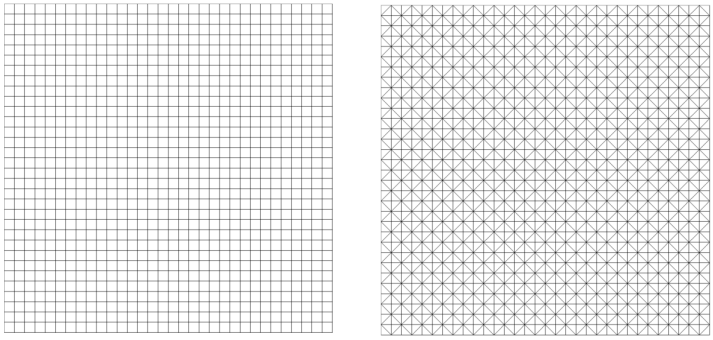

Figure 4.—Coarsened example vortex grids: Fluent/FR quadrilateral (left) and Fluent/FR triangular (right).

TABLE 2.—THE NUMBER OF DEGREES OF FREEDOM (nDOF) RUN BY EACH CODE FOR THE VORTEX PROBLEM

nDOF	Cell type	Fluent	FR
1,024	Quad	X	-
2,048	Tri	X	-
4,096	Quad	X	X
8,192	Tri	X	X
16,384	Quad	X	X
32,768	Tri	X	X
65,536	Quad	X	X
131,072	Tri	-	X
262,144	Quad	-	X
524,288	Tri	-	X

3.3 Laminar Boundary Layer on a Flat Plate

The final test problem considered is a subsonic laminar flow over a 2D flat plate (Ref. 16). The problem set up is shown in Figure 5. Boundary conditions, also shown in Figure 5, include a subsonic inflow, pressure exit, symmetry, and the flat plate modeled as an adiabatic no-slip wall. Using the grids provided by the 3rd International Workshop on High-Order CFD Methods yields $L_H = 1.25$, $L_V = 2$, and the length of the adiabatic wall as one. Simulations on a total of four structured grids were performed using the Fluent code, which used both the pressure- and density-based solvers. Table 3 lists the wall-normal spacing for the grids and Figure 6 shows a sample grid. The hpMusic code was once again used due to a lack of funding and also used the structured grids provided by the workshop. In addition, simulations were performed on five unstructured grids using the ez4d code, with the unstructured grids created by diagonalizing the structured grids used by the Fluent code. A full list of the number of degrees of freedom simulated are tabulated in Table 4. The freestream flow field for this problem was Mach 0.5, zero degrees angle of attack, and a Reynolds number of 1.0×10^6 (based on the length of the flat plate). Properties of the flow field included a Prandtl number of 0.72 and a ratio of specific heats of 1.4.

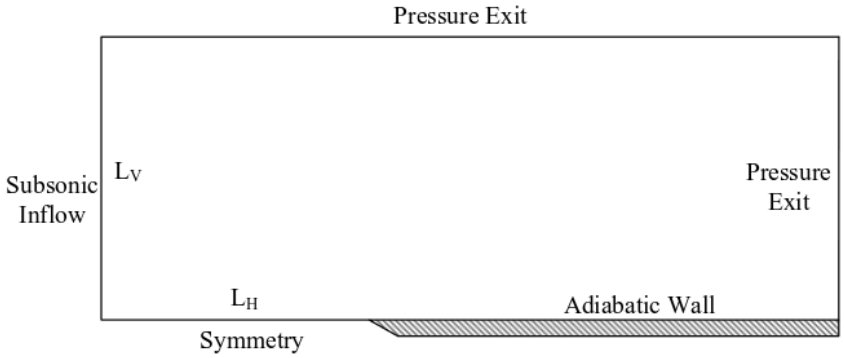

Figure 5.—Computational domain for the flat plate problem (Ref. 16).

TABLE 3.—GRID WALL-NORMAL SPACINGS RUN BY EACH CODE FOR THE FLAT PLATE PROBLEM

Δy_{wall}	Fluent	ez4d	FR
1.88×10^{-4}	X	-	X
9.38×10^{-5}	X	X	X
4.69×10^{-5}	X	X	X
2.34×10^{-5}	X	X	X
1.17×10^{-5}	-	X	-
5.86×10^{-6}	-	X	-

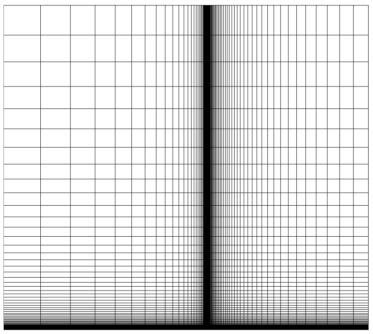

Figure 6.—Example flat plate grid with $\Delta y_{wall} = 9.38\times10^{-5}$.

TABLE 4.—THE NUMBER OF DEGREES OF FREEDOM (nDOF) RUN BY EACH CODE FOR THE FLAT PLATE PROBLEM

nDOF	Fluent	ez4d	FR
8,960	X	-	X
17,920	-	X	-
35,840	X	-	X
71,680	-	X	-
143,360	X	-	X
286,720	-	X	-
573,440	X	-	X
1,146,880	-	X	-
4,587,520	-	X	-

4.0 Results

Note that the CFL numbers and time-step sizes run by each code were small enough to ensure that the spatial discretization errors would be bigger than the temporal discretization errors for each problem. Simulations for the Ringleb and flat plate problems were run steady-state while the simulations for the vortex problem were run time-accurate.

4.1 Transonic Ringleb Flow

Figure 7 to Figure 9 show some of the entropy contours computed using the three numerical codes at the degrees of freedom outlined in Table 1. It can be seen that all three codes converge towards a constant entropy flow field, with the variation in entropy occurring along the inner wall. Due to how the curved walls were represented in the grids used by the ez4d code, the ez4d simulations were rerun with the analytical solution used as the boundary condition for the inner and outer walls. Figure 10 to Figure 12 show the entropy contours from the ez4d simulations. It can be seen that using the analytical solution at the boundaries has greatly improved the solutions compared to using the slip-wall boundary condition.

Aside from contour plots, the error associated with each converged solution was also explored. For the Ringleb problem, the error of interest was the L2 norm for entropy and was computed as follows:

$$Error_{L2(s)} = \sqrt{\frac{\sum_{i=1}^{n} \int_{A_i} \left(s_i - s_{exact,i} \right)^2 dA}{\sum_{i=1}^{n} |A_i|}} \tag{11}$$

where the entropy, s, is defined as:

$$s = \frac{p}{\rho^{\gamma}} \tag{12}$$

and the exact entropy, s_{exact}, was computed to be 0.7143 via the Ringleb problem analytical solution.

The length scale, h, was defined as a function of the degrees of freedom, which in turn is a function of the order of the numerical scheme and the number of cells or nodes per grid if the numerical scheme is cell- or node-based, respectively.

$$h = \frac{1}{\sqrt{n_{DOF}}} = \frac{1}{\sqrt{(O-1) \cdot n_{cells(nodes)}}} \tag{13}$$

Figure 13 shows the L2 norm of the entropy error for the Ringleb problem. It should be noted that Fluent was unable to get a converged solution at 12,228 degrees of freedom and therefore that data point was omitted from the figure. It can be seen that the Fluent solutions have a lower entropy error than the ez4d solutions with the slip-wall boundary condition, but have a higher entropy error than the ez4d solutions with the analytical solution boundary condition. In addition, all Fluent and ez4d solutions have a higher entropy error than the FR solutions for a given length scale. This is largely due to the fact that the FR method utilized a fourth-order scheme whereas both Fluent and ez4d utilized second-order schemes.

The Fluent and FR solutions respectively showed expected order of accuracy with second- and fourth-order convergence; however, the ez4d solutions using the slip-wall boundary condition only demonstrated first-order convergence. This is because the convergence rate of the CESE method is sensitive to the representation of the boundary curvature. Since the curved boundaries of the Ringleb problem were represented by a series of first-order lines in the grids that were used with ez4d, it prevented the code from converging at its expected second-order rate. This is mitigated when using the analytical solution boundary condition, which showed the expected second-order convergence. While the Fluent simulations also used grids with first-order representation of the curved boundaries, the numerical schemes as implemented are less sensitive to the boundary representation, partially explaining why the Fluent solutions showed second-order convergence and the ez4d solutions using the slip-wall boundary condition did not. Further, the FR solutions showed fourth-order convergence partially due to the use of grids with fourth-order representation of the curved boundaries.

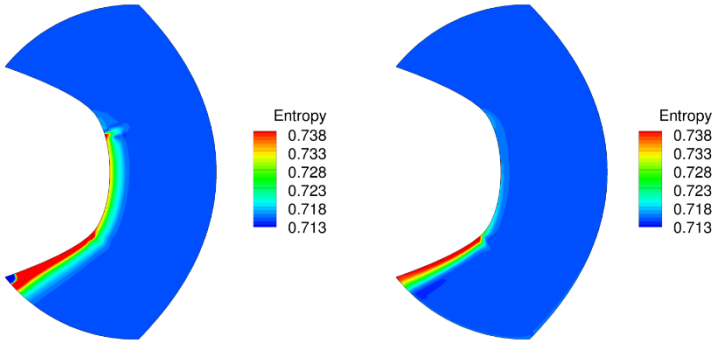

Figure 7.—Entropy contours for Fluent with 3,072 degrees of freedom (left) and ez4d with 6,144 degrees of freedom (right).

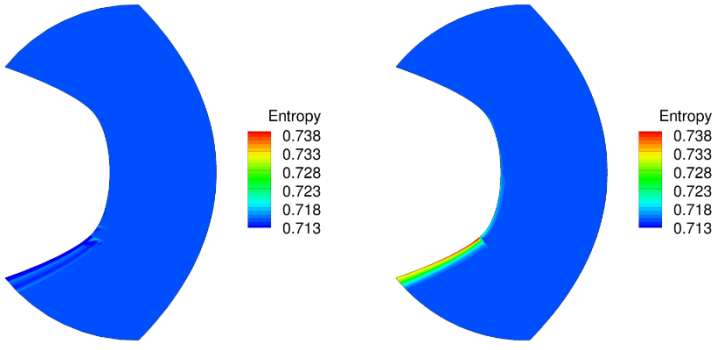

Figure 8.—Entropy contours for FR with 12,288 degrees of freedom (left) and ez4d with 24,576 degrees of freedom (right).

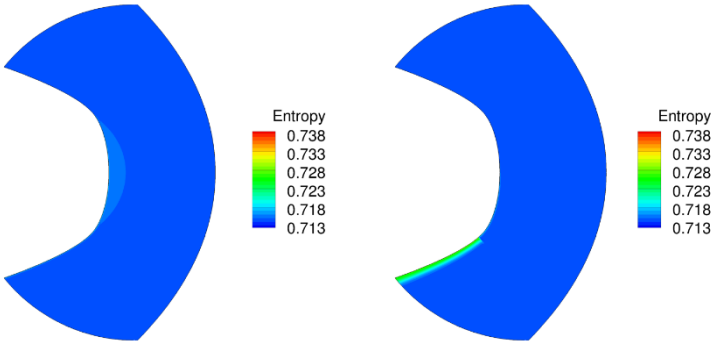

Figure 9.—Entropy contours for Fluent with 49,152 degrees of freedom (left) and ez4d with 98,304 degrees of freedom (right).

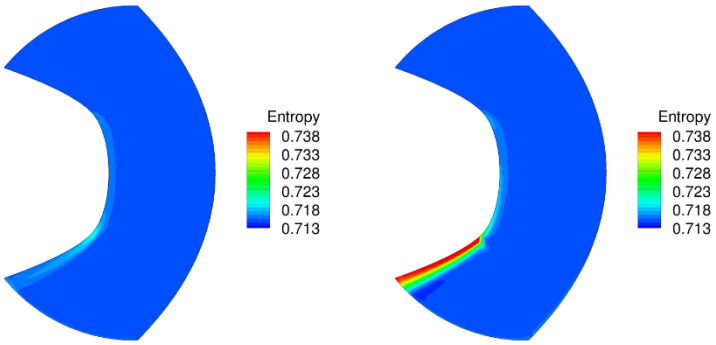

Figure 10.—Entropy contours for ez4d with 6,144 degrees of freedom using the analytical solution (left) and slip-wall (right) boundary conditions.

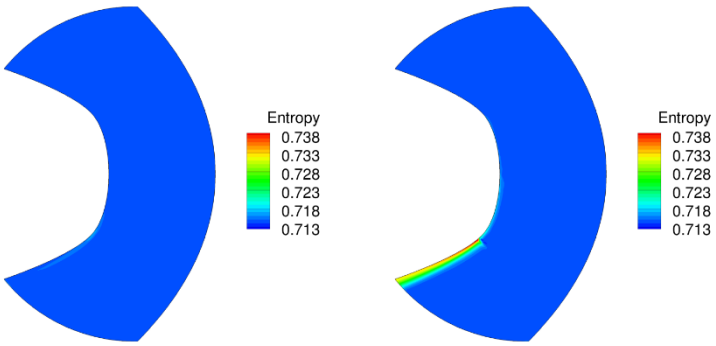

Figure 11.—Entropy contours for ez4d with 24,576 degrees of freedom using the analytical solution (left) and slip-wall (right) boundary conditions.

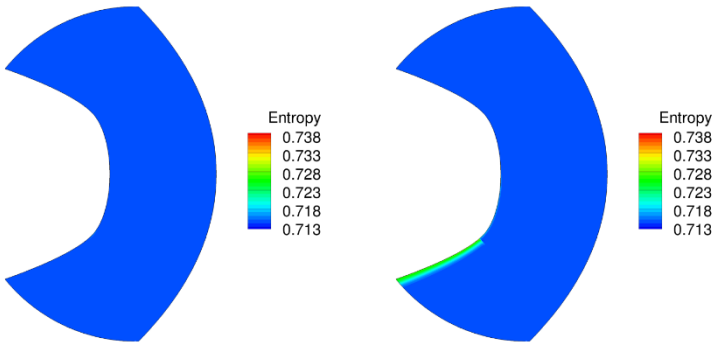

Figure 12.—Entropy contours for ez4d with 98,304 degrees of freedom using the analytical solution (left) and slip-wall (right) boundary conditions.

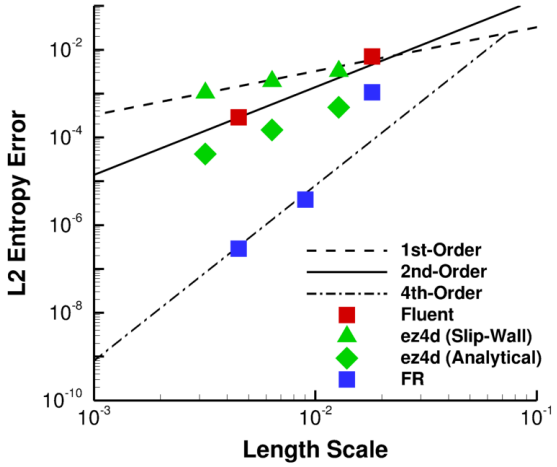

Figure 13.—L2 entropy error for the Ringleb problem.

4.2 Vortex Transport by Uniform Flow

Figure 14 through Figure 18 show some of the nondimensional u velocity contours computed using the two numerical codes at the various degrees of freedom outlined in Table 2. The ez4d solutions are absent from these comparisons as an incorrect setup could not be rectified due to a lack of time/discontinuation of funding. The u velocity contours were nondimensionalized by the freestream velocity, u_∞. It can be seen that for a given degree of freedom, the vortex tends to stretch and move downwards in the domain as the number of completed periods increases. However, increasing the number of degrees of freedom has the expected result of better preserving the exact strength and location of the vortex after completing 50 periods. The two exceptions to this are the Fluent solution with 16,384 and 32,768 degrees of freedom, which appear to dissipate the vortex completely by the time 50 periods have been completed. A closer examination of the 32,768 degrees of freedom solution reveals the highly stretched remnants of the vortex, as shown in Figure 19. For comparison, Figure 19 also shows the FR solution at the same degrees of freedom.

The errors of interest for this problem were the velocity components after the vortex had completed 50 time periods of transport. Since all boundaries are periodic and this is a purely inviscid flow, the exact solution after completing an integer number of periods is simply the initial conditions for the vortex problem. The L2 norm for the u and v velocities were defined in a similar manner to the L2 norm for the Ringleb problem.

$$Error_{L2(u)} = \sqrt{\frac{\sum_{i=1}^{n} \int_{Ai} \left(u_i - u_{initial,i}\right)^2 dA}{\sum_{i=1}^{n} |A_i|}} \tag{14}$$

$$Error_{L2(v)} = \sqrt{\frac{\sum_{i=1}^{n} \int_{Ai} \left(v_i - v_{initial,i}\right)^2 dA}{\sum_{i=1}^{n} |A_i|}} \tag{15}$$

Figure 20 shows the L2 norm of the u and v velocities for the vortex problem. On both the quadrilateral and triangular meshes, the Fluent solutions tend to be relatively flat, close to zeroth-order convergence. This is mostly due to the dissipation error maxing out the integrated L2 error and is suspected that the Fluent solutions would show an improved order of convergence if given enough degrees of freedom. The FR solutions show fourth-order convergence on both the quadrilateral and triangular meshes. All of the above trends hold true for the L2 norm of both the u and v velocities.

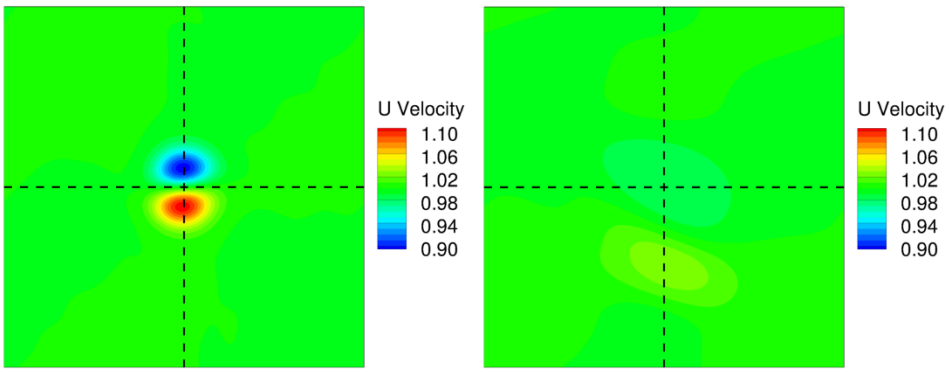

Figure 14.—u velocity contours after 1 time period (left) and 50 time periods (right) for Fluent on a quadrilateral mesh with 16,384 degrees of freedom.

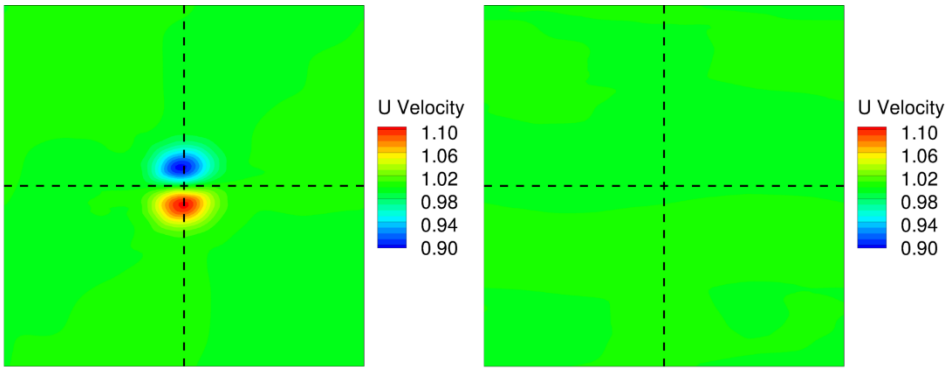

Figure 15.—*u* velocity contours after 1 time period (left) and 50 time periods (right) for Fluent on a triangular mesh with 32,768 degrees of freedom.

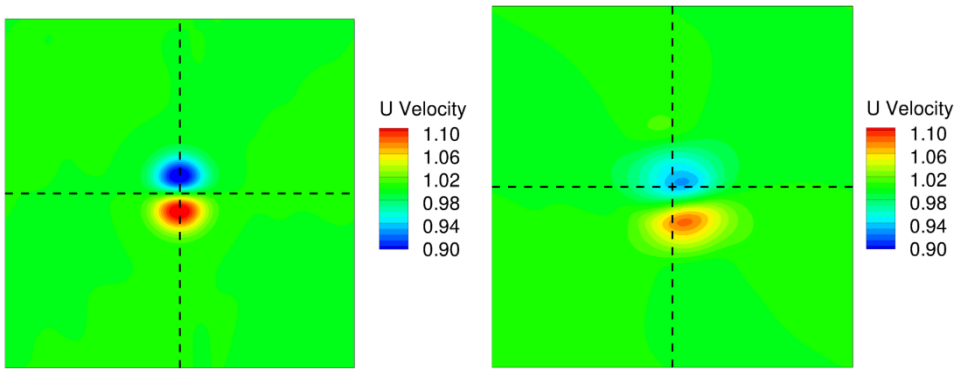

Figure 16.—*u* velocity contours after 1 time period (left) and 50 time periods (right) for Fluent on a quadrilateral mesh with 65,536 degrees of freedom.

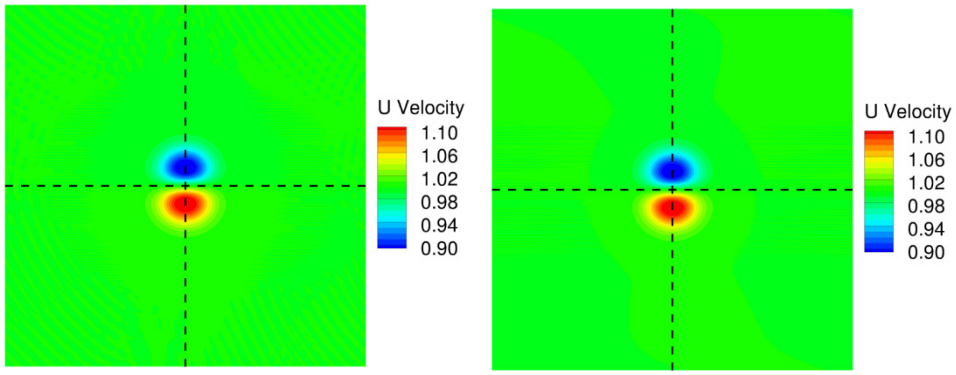

Figure 17.—*u* velocity contours after 1 time period (left) and 50 time periods (right) for FR on a quadrilateral mesh with 16,384 degrees of freedom.

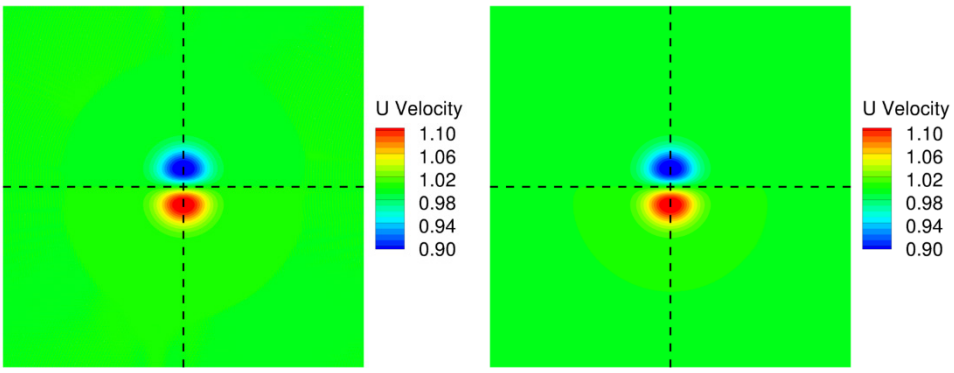

Figure 18.—*u* velocity contours after 1 time period (left) and 50 time periods (right) for FR on a triangular mesh with 524,288 degrees of freedom.

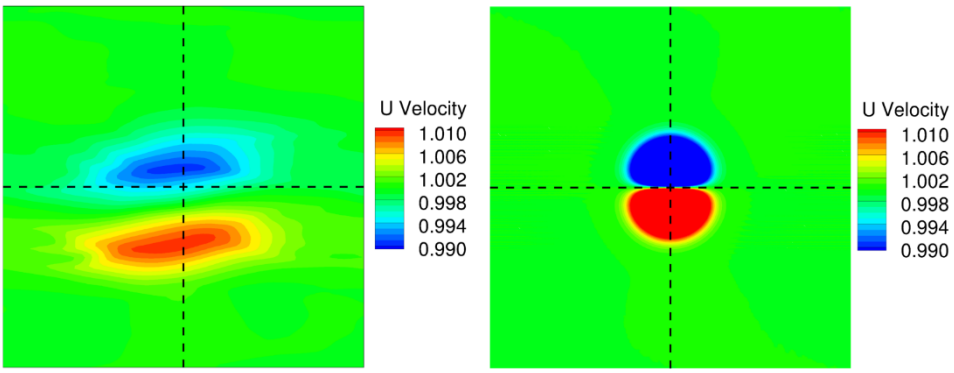

Figure 19.—*u* velocity contour after 50 time periods for Fluent (left) and FR (right) on a triangular mesh with 32,768 degrees of freedom with the contour range zoomed in.

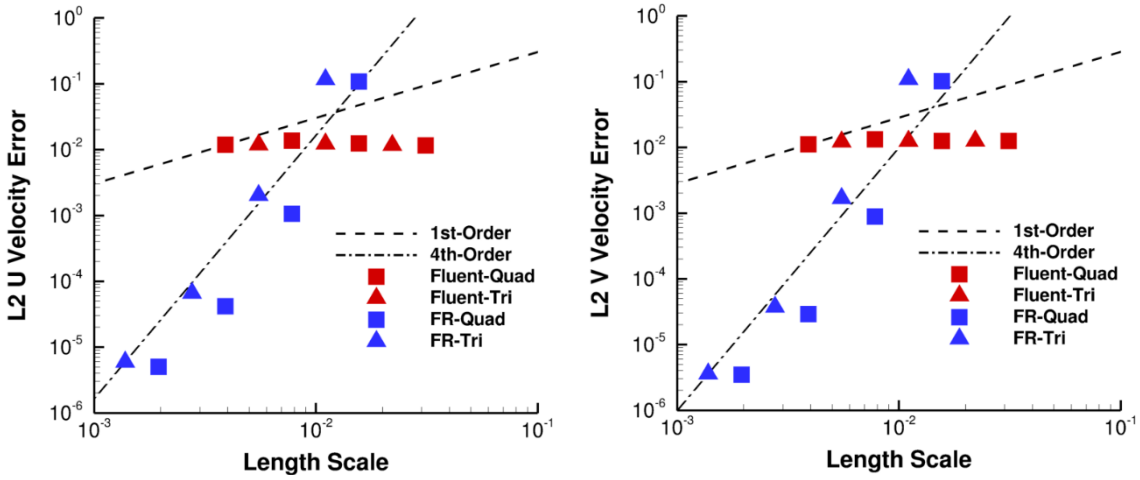

Figure 20.—L2 *u* velocity (left) and *v* velocity (right) errors for the vortex problem after 50 time periods.

4.3 Laminar Boundary Layer on a Flat Plate

For the flat plate problem, the parameter of interest was the error in the drag coefficient, c_d. Because there is no exact solution for a compressible laminar boundary layer, the exact drag coefficient was estimated by using Equation (16), which is a form of Richardson extrapolation (Refs. 17 and 18).

$$c_{d,exact} = c_{d,GL} + \frac{c_{d,GL} - c_{d,GL-1}}{2^{O(n)} - 1} \tag{16}$$

The error in the drag coefficient was then computed by Equation (17).

$$Error_{cd} = \sqrt{\frac{\left(c_d - c_{d,exact}\right)^2}{c_{d,exact}^2}} \tag{17}$$

where

$$c_{d,exact,Fluent,p} = 1.401 \cdot 10^{-3} \tag{18}$$

$$c_{d,exact,Fluent,\rho} = 1.332 \cdot 10^{-3} \tag{19}$$

$$c_{d,exact,ez4d} = 1.265 \cdot 10^{-3} \tag{20}$$

$$c_{d,exact,FR} = 1.313 \cdot 10^{-3} \tag{21}$$

The two exact drag coefficients for the Fluent code are for the pressure-based solver ($c_{d,exact,Fluent,p}$) and the density-based solver ($c_{d,exact,Fluent,\rho}$).

Figure 21 shows the error in the drag coefficient as a function of length scale. It can be seen that the Fluent pressure-based solver solutions show first-order accuracy while the Fluent density-based solver solutions show an order-of-accuracy between first- and second-order. This is in contrast to the ez4d solutions which show second-order accuracy, however, it is noted that the Fluent solutions tend to have less error for a given length scale compared to the ez4d solutions. It can also be seen that the FR solutions show the expected fourth-order accuracy. One thing to keep in mind with Figure 21 is that it is plotting error based on a solution-dependent estimate of the exact drag coefficient value, which is a value that varies between codes. With that in mind, the FR solutions are converging to the estimated exact drag coefficient value of 1.31×10^{-3} that is reported by other codes (Refs. 19 and 20). The Fluent solutions that used the density-based solver converge closer to the reported estimated exact drag coefficient than the solutions from the pressure-based solver, which in turn are closer than the ez4d solutions.

Table 5 shows the sensitivity of the estimated exact drag coefficient to the number of degrees of freedom. For the FR solutions, the estimated exact drag coefficient improves with increasing degrees of freedom and ultimately converges. The estimated exact drag coefficients for the Fluent density-based solver and ez4d solutions show initial improvement with increasing degrees of freedom. However, increasing the number of degrees of freedom beyond 143,360 for the Fluent density-based solver solutions and 1,146,880 for the ez4d solutions results in the respective codes overshooting the estimated exact drag coefficient value seen by others and do not reach a converged state. The Fluent pressure-based solver solutions predict an estimated exact drag coefficient that diverges from the value seen be others

with increasing degrees of freedom and does not reach a converged state. It is not known at this time why the Fluent and ez4d solutions behave in these ways.

Two additional metrics were used to compare the results between the three codes. First, u velocity profiles were compared, as shown in Figure 22. For reference, the incompressible Blasius solutions were also plotted, and all profiles were nondimensionalized by the freestream velocity, u_∞. It can be seen that all four CFD solutions agree well with each other. Second, the flat plate skin friction coefficient profiles were plotted, as shown in Figure 23. Just like the u velocity profiles, the Blasius solution was plotted for reference and the CFD solutions agree well with each other. These two additional metrics show that the codes are converging to the expected solution.

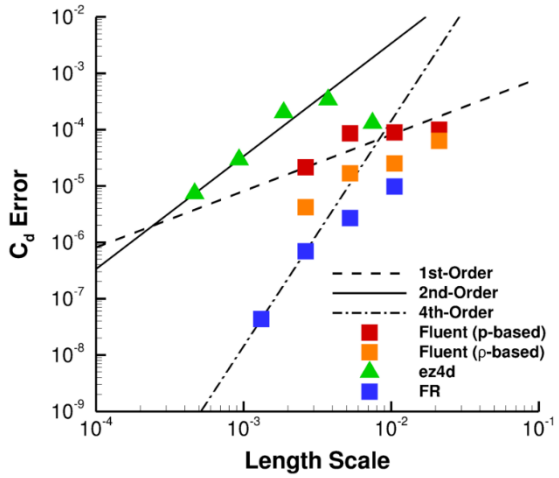

Figure 21.—Drag coefficient error for the flat plate problem.

TABLE 5.—ESTIMATED EXACT DRAG COEFFICIENT BASED ON RICHARDSON EXTRAPOLATION

nDOF	Fluent (p-based)	Fluent (ρ-based)	ez4d	FR
8,960	NA	NA	-	NA
17,920	-	-	NA	-
35,840	1.314×10^{-3}	1.278×10^{-3}	-	1.315×10^{-3}
71,680	-	-	1.596×10^{-3}	-
143,360	1.316×10^{-3}	1.318×10^{-3}	-	1.313×10^{-3}
286,720	-	-	1.458×10^{-3}	-
573,440	1.401×10^{-3}	1.332×10^{-3}	-	1.313×10^{-3}
1,146,880	-	-	1.287×10^{-3}	-
4,587,520	-	-	1.265×10^{-3}	-

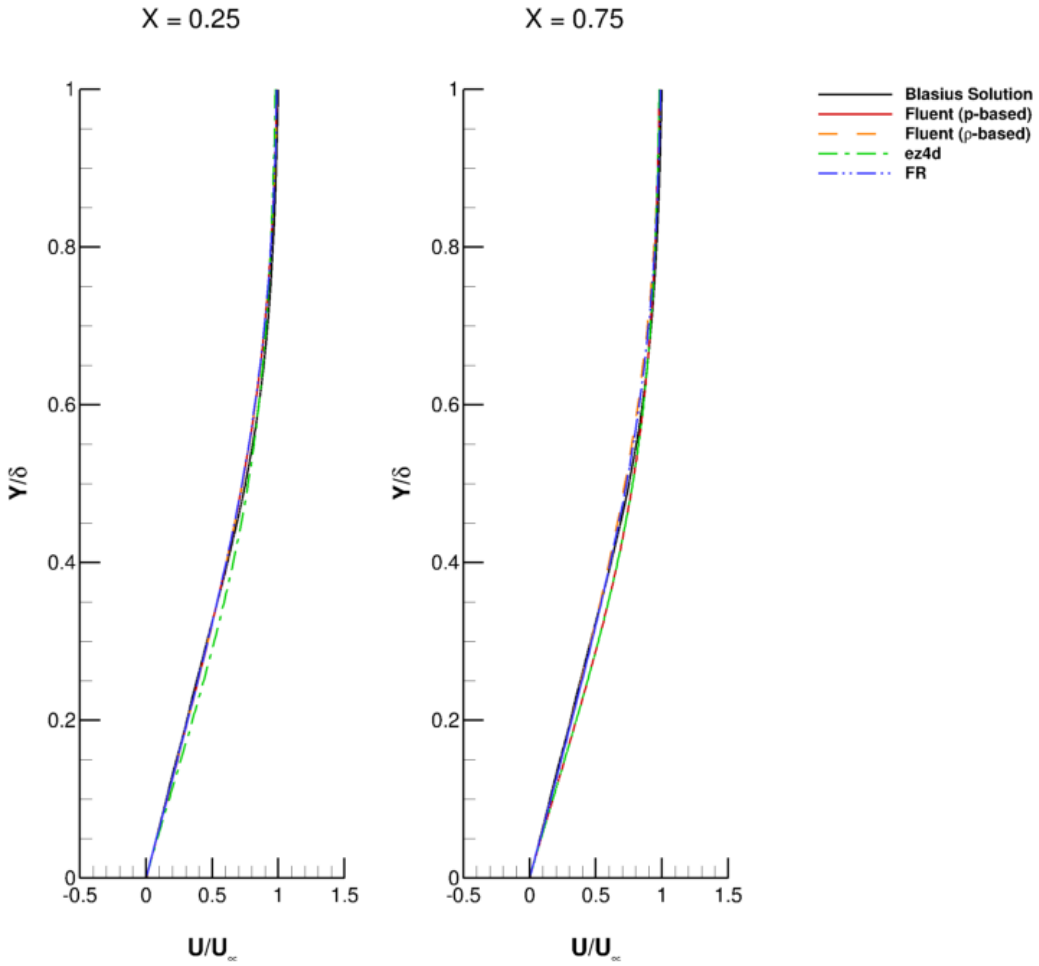

Figure 22.—Nondimensional *u* velocity profiles for ez4d with 1,146,880 degrees of freedom, Fluent with 573,440 degrees of freedom, and FR with 573,440 degrees of freedom.

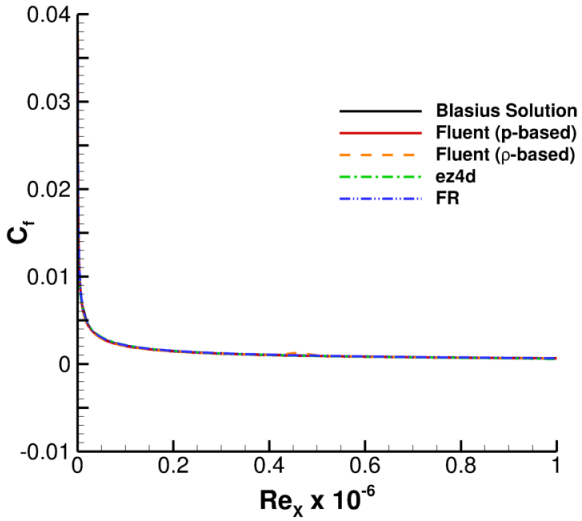

Figure 23.—Skin friction coefficient profiles for ez4d with 1,146,880 degrees of freedom, Fluent with 573,440 degrees of freedom, and FR with 573,440 degrees of freedom.

5.0 Conclusions

To conclude, several different CFD codes were run on three different high-order workshop benchmark problems to compare solution accuracy between the codes. Converged solutions produced by the ANSYS Fluent code had lower errors compared to converged solutions produced by the ez4d code for the Ringleb and flat plate problems. Both the Fluent and ez4d converged solutions had higher errors for all benchmark problems presented in this paper when compared to the converged solutions from the FR codes for a given length scale. Whereas both Fluent and ez4d utilized second-order schemes, the FR codes utilized a fourth-order scheme, explaining why they outperformed both Fluent and ez4d in terms of error at the same number of degrees of freedom.

References

1. Wang, Z.J., Fidkowski, K.J., Abgrall, R., Bassi, F., Caraeni, D., Cary, A., Deconinck, H., Hartmann, R., Hillewaert, K., Huynh, H. T., Kroll, N., May, G., Persson, P-O., van Leer, B, and Visbal, M., "High-Order CFD Methods: Current Status and Perspective," *International Journal for Numerical Methods in Fluids*, No. 72, 2013, pp. 811–845.
2. ANSYS Inc., "ANSYS Fluent Flow Solver, Version 17.2," 2016, Canonsburg, PA.
3. Roe, P.L., "Characteristic-Based Schemes for the Euler Equations," *Annual Review of Fluid Mechanics,* Vol. 18, 1986, pp. 337–365.
4. Rauch, R.D., Batira, J.T., and Yang, N.T.Y., "Spatial Adaptation Procedures on Unstructured Meshes for Accurate Unsteady Aerodynamic Flow Computations," Tech. Rep. AIAA 91-1106, 1991.
5. "ANSYS Fluent Theory Guide, Release 17.2," ANSYS Inc., Canonsburg, PA, 2016.
6. Chang, S.-C., "The Method of Space-Time Conservation Element and Solution Element – A New Approach for Solving the Navier-Stokes and Euler Equations," *Journal of Computational Physics*, Vol. 119, No. 2, 1995, pp. 295–325.
7. Chang, S.-C., Wang, X.-Y., and Chow, C.-Y., "The Space-Time Conservation Element and Solution Element Method – A New Resolution and Genuinely Multidimensional Paradigm for Solving Conservation Laws," *Journal of Computational Physics*, Vol. 156, No. 1, 1999, pp. 89–136.
8. Chang, S.-C., "A New Approach for Constructing Highly Stable High Order CESE Schemes," Tech. Rep. AIAA 2010-543, January 2010.
9. Chang, C.-L., "Time-Accurate, Unstructured-Mesh Navier-Stokes Computations with the Space-Time CESE Method," Tech. Rep. AIAA 2006-4780, July 2006.
10. Chang, C.-L., Venkatachari, B., and Cheng, G., "Time-Accurate Local Time Stepping and High-Order Space-Time CESE Methods for Multi-Dimensional Flows with Unstructured Meshes," Tech. Rep. AIAA 2013-3069, June 2013.
11. Huynh, H. T., "A Flux Reconstruction Approach to High-Order Schemes Including Discontinuous Galerkin Methods," Tech. Rep. AIAA 2007-4079, June 2007.
12. Huynh, H. T., Wang, Z.J., and Vincent, P.E., "High-Order Methods for Computational Fluid Dynamics: A Brief Review of Compact Differential Formulations on Unstructured Grids," *Computer and Fluids*, Vol. 98, July 2014, pp. 209–220.
13. Huynh, H.T., "Problem C1.2. Ringleb Problem," 3rd International Workshop on High-Order CFD Methods, URL: https://www1.grc.nasa.gov/wp-content/uploads/case_c1.1.pdf [cited 23 July 2021].
14. Caraeni, D., "Problem C1.6. Vortex transport by uniform flow," 3rd International Workshop on High-Order CFD Methods, URL: https://www1.grc.nasa.gov/wp-content/uploads/case_c1.4.pdf [cited 23 July 2021].

15. Jia, F., Ims, J., Wang, Z.J., Kopriva, J., and Laskowski, G.E., "Evaluation of Second- and High-Order Solvers in Wall-Resolved Large-Eddy Simulation," *AIAA Journal,* December 2018, pp. 1–13.
16. Bassi, F, and Darmofal, D., "Problem C1.4. Laminar Boundary Layer on a Flat Plate," 3rd International Workshop on High-Order CFD Methods, URL: https://www1.grc.nasa.gov/wp-content/uploads/case_c1.3.pdf [cited 23 July 2021].
17. Richardson, L.F., "The Approximate Arithmetical Solution by Finite Differences of Physical Problems including Differential Equations, with an Application to the Stresses in a Masonry Dam," *Philosophical Transactions of the Royal Society A*, Vol. 210, Issue 459-470, January 1911, pp. 307–357.
18. Richardson, L.F., and Gaunt, J.A., "The Deferred Approach to the Limit," *Philosophical Transactions of the Royal Society A*, Vol. 226, Issue 636-646, January 1927, pp. 299–349.
19. Navah, F., Vermeire, B., and Nadarajah, S., "Flat Plate Boundary Layer – Problem C1.3," 3rd International Workshop on High-Order CFD Methods, URL: https://www1.grc.nasa.gov/wp-content/uploads/C1.3_McGill.pdf [cited 23 July 2021].
20. Ferrero, A. and Larocca, F., "Case C1.3: Flat Plate Boundary Layer," 3rd International Workshop on High-Order CFD Methods, URL: https://www1.grc.nasa.gov/wp-content/uploads/C1.3_Torino.pdf [cited 23 July 2021].